ORIGINAL PAPER - CONDENSED MATTER

Synthesis of Ni-based fluoroperovskites by solvent-free mechanochemical reaction

Jin San Choi[1] · Muhammad Sheeraz[1] · Fazli Akram[1] · Hyoung-Su Han[2] · Jae-Shin Lee[2] · Chang Won Ahn[1] · Tae Heon Kim[1]

Abstract

We realized fluoride perovskites ANiF$_3$ (A = Na, K, and Ag) incorporating a transition-metal Ni element using solvent-free mechanochemical reaction processes. Methodologically, two different synthetic routes were devised based on the conventional mechanical grinding and the planetary ball milling techniques. The structural characteristics of the as-synthesized fluoroperovskite powders were determined by powder X-ray diffraction measurements and subsequent Rietveld refinement analyses. The band gaps and the chemical compositions of the ANiF$_3$ powders were also examined by ultraviolet–visible absorption measurements and element-specific energy dispersive X-ray spectroscopy, respectively. The goodness of factors of our refinements revealed that the high-energy planetary ball milling was more beneficial than the conventional grinding method in achieving a perovskite ANiF$_3$ phase mechanically. We found that the degree of mechanochemical reaction to form the perovskite phase depended on the crystal structure. With the fitted lattice parameters of the fluoride perovskites, we discussed how a structural modification induced by cation non-stoichiometry affected the stabilization of the fluoroperovskite materials via the mechanochemical synthesis.

Keywords Mechanochemistry · Fluoroperovskite · Powder · X-ray diffraction

1 Introduction

For several decades, perovskite ABX_3 materials, which generally consist of two cations (A and B) and one chalcogen or halogen anion (X), have attracted tremendous attention to the associated fields of condensed-matter physics, materials science, and physical chemistry due to the large variety of the fascinating physical properties [1, 2]. In the perovskite oxides ABX_3 (X = O; ABO$_3$), which contains a BO$_6$ octahedron in the pseudocubic unit cell, intriguing physical phenomena such as superconductivity [3, 4], metal-to-insulator phase transition [5, 6], ferroelectricity [7, 8], piezoelectricity [9–11], multiferroicity [12, 13], thermoelectricity [14, 15], magnetoresistance [16], ionic conductivity [17, 18],

photovoltaic effects [19, 20], and electrocatalysis [21, 22] have been extensively reported. For the perovskite oxides, the thermodynamic phase stability and their physical properties are well known to be very susceptible to structural distortion, thereby a change in the crystallographic symmetry [23]. In general, such a distortion in a perovskite ABO$_3$ lattice can be described using the Goldschmidt tolerance factor t and octahedral factor μ, which are closely related to the tilting and the rotation of the BO$_6$ octahedron [1, 2, 24, 25]. For perovskite ABX_3, t and μ can be represented with the following equations [1, 2]:

$$\text{Tolerance factor } t = \frac{R_A + R_X}{\sqrt{2}(R_B + R_X)}, \tag{1}$$

$$\text{Octahedral factor } \mu = \frac{R_B}{R_X}, \tag{2}$$

where R_A, R_B, and R_X are the ionic radii of the A-site cation, the B-site cation, and the X anion, respectively.

Fluoroperovskites ABX_3 (X = F; ABF$_3$), where the A-site cation is usually monovalent (e.g., Na$^+$, K$^+$, and Ag$^+$) and

✉ Tae Heon Kim
  thkim79@ulsan.ac.kr

[1] Department of Physics and Energy Harvest-Storage Research Center (EHSRC), University of Ulsan, Ulsan 44610, Republic of Korea

[2] School of Materials Science and Engineering, University of Ulsan, Ulsan 44610, Republic of Korea

the B-site cation is a multivalent transition-metal element, are promising candidate materials with multi-functionality in the electrical, magnetic, optical, and ionic transport properties [26–28]. Furthermore, the perovskite fluorides exhibit not only excellent electrochemical properties (e.g., electrocatalytic performance) attributed to the strong electronegativity of the F^- ion but also robust ionicity due to the weak bond strength between the B-site transition-metal cation and the F^- anion [22]. Nevertheless, previous works on these attractive physical properties are rare due to the challenge in synthesizing fluoroperovskite compounds [29]. Note that fluoride perovskites are structurally unstable in air because the fluoroperovskites easily react with water molecules or oxygen gas in the atmosphere, which results in the formation of secondary phases [30–34]. Owing to the vulnerability of fluoroperovskites to humidity [32], either chemical solvents or sealed/isolated containers have been commonly used to avoid the introduction of water molecules from air during their synthesis [34–38]. However, a synthetic route to achieve the fluoroperovskite phase free from a solvent has not been examined systematically, yet [38–40].

In this work, we demonstrate the realization of fluoroperovskite phases through a solvent-free mechanochemical reaction [41–45]. Three Ni-based perovskite fluoride compounds, NaNiF$_3$, KNiF$_3$, and AgNiF$_3$, were attained in a powder form using the mechanical-milling-based synthetic methods. We found the formation of the fluoroperovskite phase to be easier via the high-energy planetary ball milling rather than the conventional grinding in a mortar with a pestle. The structural properties, the electronic band gaps, and the chemical compositions of the as-prepared fluoroperovskite powders were characterized using X-ray diffraction (XRD), ultraviolet (UV)–visible spectroscopy, and energy dispersive X-ray spectroscopy (EDS), respectively. We will also discuss the phase stability of the fluoroperovskite materials in terms of structural distortions based on the calculated t values of the bulk NaNiF$_3$, KNiF$_3$, and AgNiF$_3$ compounds.

2 Experiments

For our aim to realize Ni-based fluoroperovskite ANiF$_3$ (A = Na, K, and Ag) compounds experimentally, we developed two kinds of solvent-free synthetic procedures including different mechanochemical reaction techniques: one was conventional mechanical grinding (named as method 1) and the other was planetary ball milling (named as method 2). In the first approach to fabricate ANiF$_3$ powders, we weighed and mixed two raw powders of AF [A = Na, K, and Ag; NaF (> 99%), KF (> 99.0%), and AgF (99%), respectively], and NiF$_2$ (≥ 95%) according to the molar ratio (all powder reagents were purchased from Sigma Aldrich). Then, ~ 3 ml of anhydrous ethyl alcohol (C$_2$H$_5$OH) was inserted into the mixed powders with no additional solvent to produce a slurry. The powder-mixture slurry was blended in a mortar with a pestle for the mechanochemical reaction for about 15 min. After the mechanical grinding, the composite powder was annealed in a muffle furnace at 250 °C for 2 h for a further reaction via calcination. More details on the first synthetic route are shown in Supplementary Fig. S1. In the second process via planetary ball milling (Supplementary Fig. S2), the weighed powder mixture of AF and NiF$_2$ was ground with C$_2$H$_5$OH (~ 3 ml) in a mortar until it was dry (~ 15 min). We moved the mixed powders of 1 g with 10 g of zirconia balls (diameter: 5 mm) into an autoclave and then mounted the autoclave to a high-energy ball milling machine (Pulverisette 7 Micro Mill, Fritsch, Germany). For a mechanochemical reaction, the powder mixture in the autoclave was blended at a rotation speed of 900 rpm and a revolution speed of 1800 rpm for 30 min.

Table 1 Calculated lattice constants and goodness of fit via the Rietveld refinements of the XRD patterns of (a) NaNiF$_3$, (b) KNiF$_3$, and (c) AgNiF$_3$ powders synthesized by methods 1 and 2

Materials	Conventional mechanical grinding (method 1)		Planetary ball milling (method 2)		Reference		
	Lattice constant (Å)	Goodness of fit (χ^2)	Lattice constant (Å)	Goodness of fit (χ^2)	Structure	Lattice constant (Å)	References
NaNiF$_3$	a = 5.38 b = 5.55 c = 7.72	3.17	a = 5.38 b = 5.55 c = 7.72	2.59	Orthorhombic ($Pnma$)	a = 5.36 b = 5.52 c = 7.69	[59]
KNiF$_3$	a = 4.03 b = 4.03 c = 4.03	9.28	a = 4.03 b = 4.03 c = 4.03	3.93	Cubic ($Pm\overline{3}m$)	a = 4.01	[65]
AgNiF$_3$	a = 3.83 b = 3.92 c = 3.93	2.55	a = 3.83 b = 3.92 c = 3.93	2.45	Cubic ($Pm\overline{3}m$)	a = 3.93	[66]

Table 2 Direct band gaps of the as-synthesized $NaNiF_3$ and $KNiF_3$ powders estimated by linear fits of the Tauc plots in Fig. 3

Materials	Conventional mechanical grinding (method 1)	Planetary ball milling (method 2)	Reference	
	Band gap E_g (eV)	Band gap E_g (eV)	Direct band gap (eV)	References
$NaNiF_3$	5.52	5.45	N/A	N/A
$KNiF_3$	5.29	5.23	5.59	[51]

The structural properties of the as-synthesized Ni-based fluoroperovskite $ANiF_3$ (A = Na, K, and Ag) powders were analyzed using a 4-circle X-ray diffractometer [wavelength λ = 1.5406 Å (Cu Kα₁), D8 Advance, Bruker, Germany], and

the lattice parameter of each phase in the $ANiF_3$ powders was extracted by fitting the obtained XRD $\theta - 2\theta$ spectra via a Rietveld refinement. The fitting process was implemented using the refinement program FullProf Suite, while adjusting the peak-shape parameters and crystal-structure parameters continuously [46–48]. To evaluate the goodness of the fitted results in the Rietveld refinement, we also obtained the goodness of factor (χ^2), which was extracted from the difference ($Y_{obs} - Y_{calc}$) between the observed XRD spectra (Y_{obs}) and the simulated XRD patterns (Y_{calc}) via a fit. The refined lattice parameters (i.e., a, b, and c) of the fluoroperovskite $ANiF_3$ phase in the as-synthesized composite powders and the corresponding χ^2 values are summarized in Table 1.

The electronic band gaps of the as-synthesized fluoroperovskite powders were quantified using UV–visible absorption spectroscopy. An ultraviolet–visible spectrophotometer (UV–Vis, V-670, JASCO, Japan) was used to measure the

Fig. 1 Rietveld refinement of the XRD patterns of **a** $NaNiF_3$, **b** $KNiF_3$, and **c** $AgNiF_3$ ceramic powders prepared by method 1. The observed XRD profiles of the $ANiF_3$ powder are represented by black circles. The XRD fitted lines of the calculated (Y_{cal}) and the difference between the observed and the calculated ($Y_{obs} - Y_{cal}$) XRD patterns are represented by red and blue lines, respectively. We labeled the positions of the Bragg peaks of **a** orthorhombic $NaNiF_3$, **b** cubic $KNiF_3$, and **c** pseudocubic $AgNiF_3$ in the XRD $\theta - 2\theta$ scans of the as-prepared Ni-based fluoroperovskites. The olive and the orange tick lines are labeled to the secondary peaks of **a** NiF_2 and NaF in $NaNiF_3$ and **b** NiF_2 and Ag in $AgNiF_3$, respectively
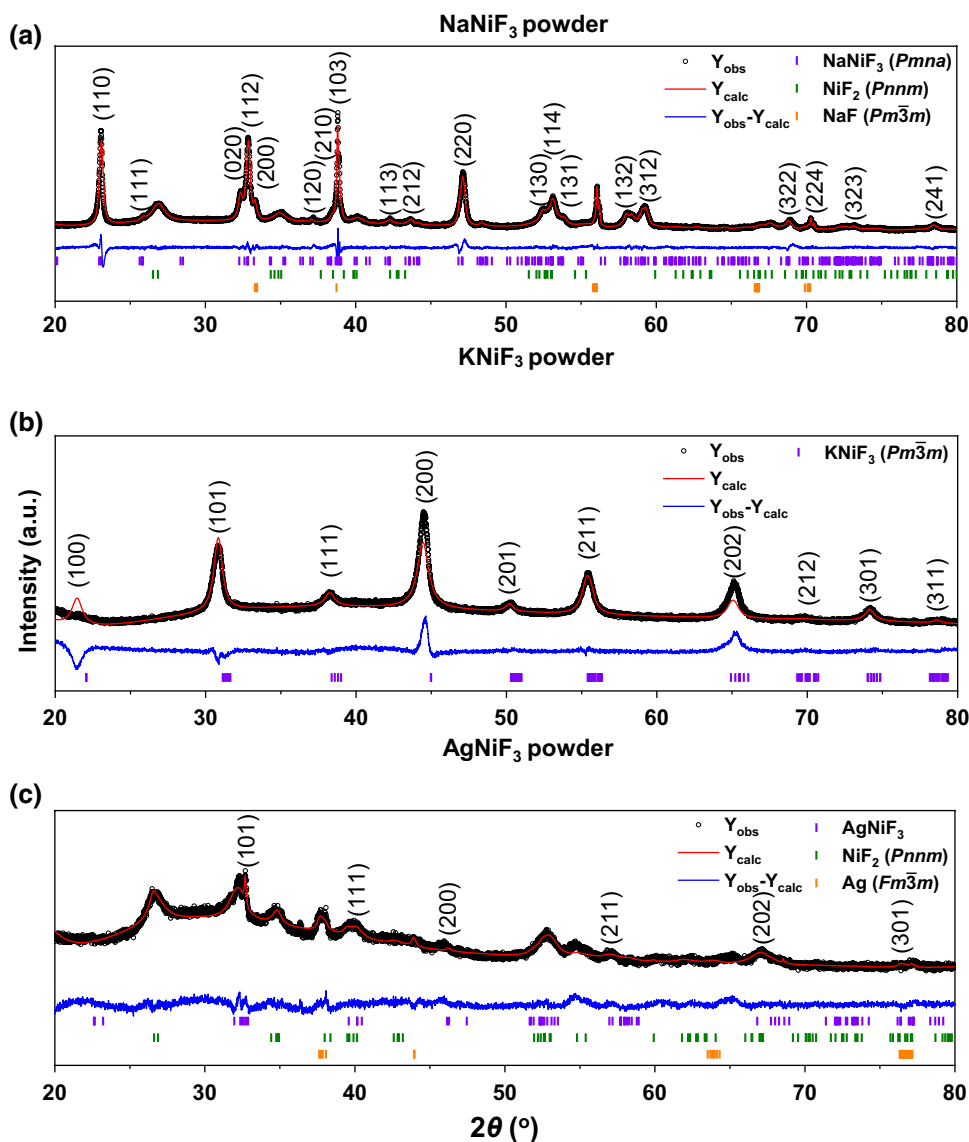
UV–visible absorption spectra of our fluoride perovskite powders. The spectral data were collected in the wavelength range between 200 and 2500 nm. The direct band gaps of the powder samples were determined using Tauc plots, and the estimated band gaps are shown in Table 2.

The chemical stoichiometry of the as-synthesized Ni-based fluoroperovskite ANiF$_3$ ($A =$ Na, K, and Ag) powders was identified by EDS measurements. For the EDS analyses, a field emission scanning electron microscopy (FE-SEM; JSM-7600, JEOL, Japan) with an EDS detector was used. Ahead of the SEM–EDS experiments, we coated the ANiF$_3$ powders with gold by direct current (DC) sputtering and placed them on carbon tapes. Then, we performed EDS measurements at target areas on the powder specimens. The atomic percentages of A, Ni, and F elements in the as-prepared ANiF$_3$ ($A =$ Na, K, and Ag) powders were estimated by analyzing the corresponding A-K edge, Ni-K edge, and F-K edge EDS signals, respectively.

3 Results and discussion

Figure 1 shows XRD $\theta - 2\theta$ scans of the as-prepared Ni-based fluoroperovskite ANiF$_3$ ($A =$ Na, K, and Ag) powders based on conventional mechanical grinding (i.e., method 1). As shown in Fig. 1b, KNiF$_3$ powders were structurally in a single perovskite phase with a cubic lattice constant of 4.03 Å, which is close to the bulk reference value of 4.01 Å (Table 1). By contrast, NaNiF$_3$ and AgNiF$_3$ powders incorporated not only the primary fluoroperovskite but also the secondary phases (e.g., the residues of the starting materials and the by-products) (Fig. 1a, c). For the NaNiF$_3$ composite, the raw materials, NaF and NiF$_2$ powders, remained without further reaction to the perovskite phase. Moreover, for the AgNiF$_3$ composite, some Ag$^+$ ions in the initial reagent of AgF were reduced to Ag metal after the mechanochemical reaction. Considering that the ionization energy of the

Fig. 2 Rietveld refinement of the XRD patterns of **a** NaNiF$_3$, **b** KNiF$_3$, and **c** AgNiF$_3$ ceramic powders prepared by method 2. The observed XRD profiles of the ANiF$_3$ powder are represented by black circles. The XRD fitted lines of the calculated (Y_{cal}) and the difference between the observed and the calculated ($Y_{obs} - Y_{cal}$) XRD patterns are represented by red and blue lines, respectively. We labeled the positions of the Bragg peaks of **a** orthorhombic NaNiF$_3$, **b** cubic KNiF$_3$, and **c** pseudocubic AgNiF$_3$ in the XRD $\theta - 2\theta$ scans of the as-prepared Ni-based fluoroperovskites. The olive and the orange tick lines are labeled to the secondary peaks of **a** NiF$_2$ and NaF in NaNiF$_3$ and **b** NiF$_2$ and AgF in AgNiF$_3$, respectively
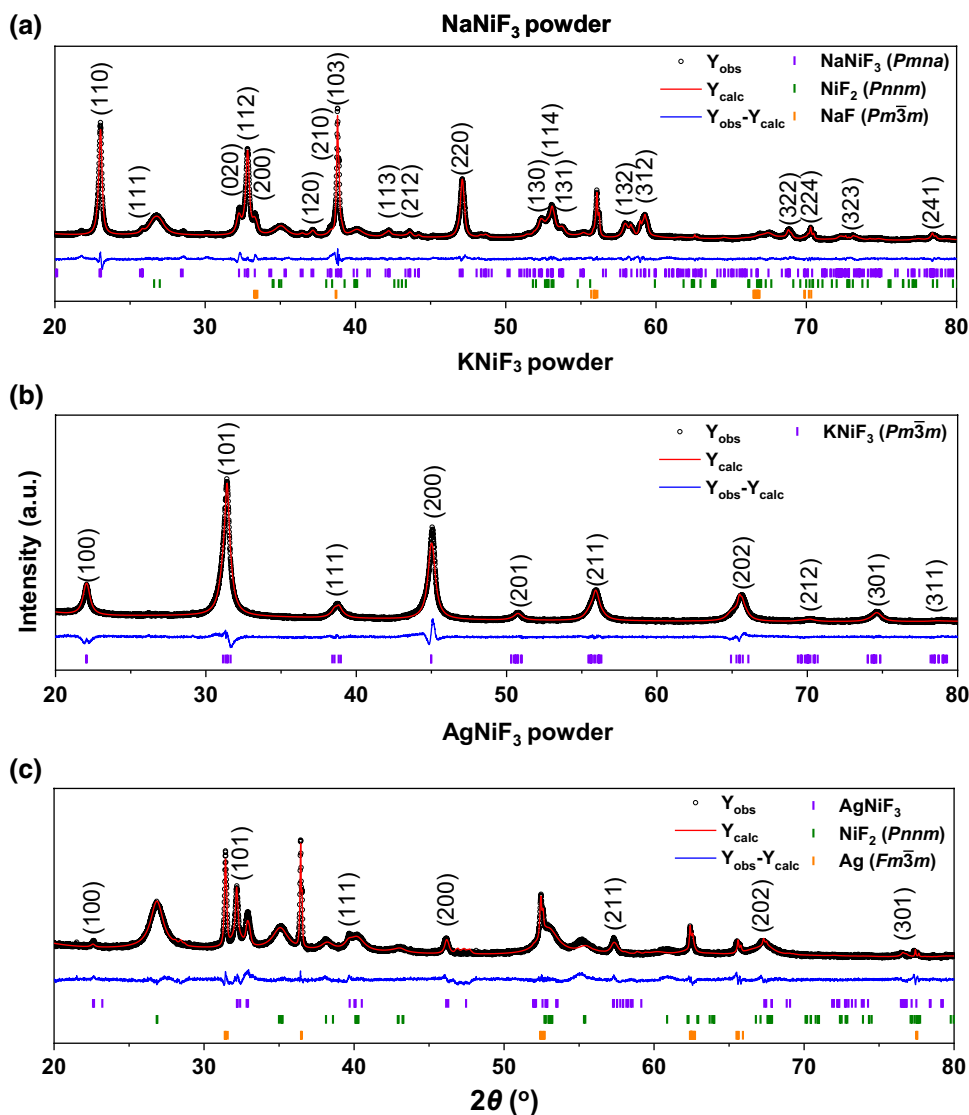
transition-metal Ag is much larger than those of alkali metals (i.e., Na and K) [49], the reduction of Ag^+ ions to Ag metal would be energetically more favorable than the formation of the fluoroperovskite $AgNiF_3$ via a chemical reaction.

To promote the mechanochemical reactivity further and to yield a larger amount of fluoroperovskite $ANiF_3$ (A = Na, K, and Ag) as the product, we synthesized Ni-based fluoride perovskite powders by solvent-free planetary ball milling (i.e., method 2). We first identified that the fluoride perovskite structure was major in the as-prepared $NaNiF_3$ and $KNiF_3$ powders (Fig. 2a, b). Seemingly, the obtained powder-XRD results of the $NaNiF_3$ and $KNiF_3$ composite compounds were comparable to the XRD spectra of the $NaNiF_3$ and $KNiF_3$ powders synthesized by method 1. Interestingly, a perovskite phase in the as-prepared $AgNiF_3$ powders was more evident, exhibiting a higher peak intensity compared with that in the $AgNiF_3$ powders synthesized by method 1 (Fig. 2c), although the residues of the initial AgF and NiF_2 powders still existed. We note that no Ag metal was observed. This implies that the high-energy ball milling could impede the reduction of Ag^+ ions, thereby facilitating the chemical reaction of AgF and NiF_2 to form the fluoroperovskite $AgNiF_3$ [50].

Figure 3 presents the UV–visible absorption spectra of our $NaNiF_3$ (orange) and $KNiF_3$ (purple) powders synthesized by methods 1 (solid lines) and 2 (dotted lines). For the $AgNiF_3$ powders, the measured absorption spectrum was not convincing due to the large amounts of secondary phases (i.e., NiF_2 and AgF) (not shown here). To estimate the direct
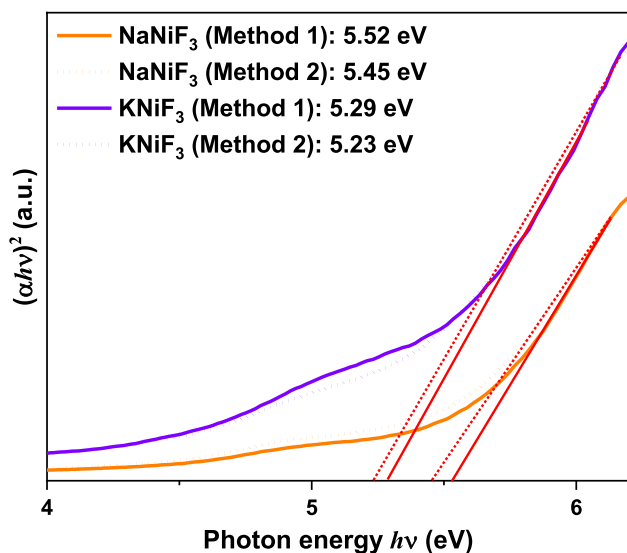

Fig. 3 Tauc plots of the UV–visible absorption spectra of $NaNiF_3$ (marked in orange) and $KNiF_3$ (marked in purple) powders synthesized by method 1 (solid lines) and method 2 (dotted lines). The direct band gaps of fluoroperovskite $NaNiF_3$ and $KNiF_3$ were estimated by linear fits (red lines) to the obtained Tauc plots

band gaps (E_g) of the as-synthesized fluoroperovskite powders, we plotted $(\alpha h\nu)^2$ as a function of the photon energy $h\nu$ (Tauc plot), where α is the absorption coefficient of the specimen. With linear fits (red lines) to the Tauc plots, the value of E_g for the $NaNiF_3$ and the $KNiF_3$ powders were found to be 5.52 (5.45) and 5.29 (5.23) eV for the method 1 (method 2), respectively. For $KNiF_3$, the obtained E_g values were comparable to the values (~5.59 eV) predicted by theoretical calculations (summarized in Table 2) [51]. Note that E_g is very susceptible to structural distortion in a solid [5, 6]. When the crystal structure is distorted, E_g in the electronic structure commonly increases due to bandwidth narrowing [5, 6]. Considering that $NaNiF_3$ was more structurally distorted with a smaller tolerance factor (t ~ 0.952) than $KNiF_3$ (t ~ 1.04) [2], the obtained E_g of $NaNiF_3$ should be larger than that of $KNiF_3$ for both methods 1 and 2.

To understand a possible origin of the difference in the formation of the perovskite phase in $ANiF_3$ (A = Na, K, and Ag) powders, we carried out EDS analyses to examine the chemical stoichiometry of the $ANiF_3$ powders synthesized by method 2 (Fig. 4). From the obtained EDS spectra, we found that the $NaNiF_3$ and the $KNiF_3$ powders were slightly Ni-deficient, deviating from a stoichiometric composition (Fig. 4a, b). In contrast, $AgNiF_3$ powders appeared to be very Ag-deficient (Ni-rich) locally (Fig. 4c). Note that the atomic percentages of A, Ni, and F correspond to 20, 20, and 60, respectively, for the stoichiometric fluoroperovskite $ANiF_3$ compound. A comparison between the Ag and the Ni contents showed that the molar concentration of Ag atoms was approximately an order of magnitude smaller than that of Ni atoms. Note that the accuracy of the obtained atomic concentrations in the EDS measurements was approximately ± 2–5% [52, 53]. Although the presence of a NiF_2 residue in the $AgNiF_3$ composite powders has been considered, such a difference in the atomic percentage between Ag and Ni ions is too huge compared with other fluoroperovskite materials, indicating that the fluoride perovskite $AgNiF_3$ should be Ag-deficient, that is, $Ag_{1-x}NiF_{3-\delta}$.

Distortions of the NiF_6 octahedral structure in fluoroperovskite $ANiF_3$ (A = Na, K, and Ag) would be closely associated with the phase formation during the synthesis of perovskite fluorides. Note that the tolerance factors t_{NaNiF3}, t_{KNiF3}, and t_{AgNiF3} of bulk $NaNiF_3$ (orthorhombic, $Pnma$), $KNiF_3$ (cubic, Pm–$3m$), and $AgNiF_3$ (cubic, Pm–$3m$) with stoichiometric compositions are 0.952, 1.04, and 0.987, respectively [2]. The octahedral factor μ is identical to 0.519 for Ni-based fluoroperovskites because all compounds of $NaNiF_3$, $KNiF_3$, and $AgNiF_3$ possess the same B-site Ni^{2+} ions and fluorine F^- ions [2]. We stress that a tolerance factor of less than 1 in a perovskite structure is mainly attributed to distortions (i.e., octahedral tilting and rotation) of the octahedral network/coordinate [25, 54–56]. With octahedral distortions, the original crystal structure of a cubic perovskite (Pm–$3m$)

Fig. 4 Surface field emission scanning electron microscopy (FE-SEM) images of the corresponding energy dispersive spectroscopy (EDS) spectra of **a** $NaNiF_3$, **b** $KNiF_3$, and **c** $AgNiF_3$ ceramic powders. The atomic percentages of Na, K, Ag, Ni, and F ions in the $NaNiF_3$, $KNiF_3$, and $AgNiF_3$ ceramic powders are shown

(a) NaNiF₃ powder

Element	Atomic%
Na *K*	19.21
Ni *K*	11.63
F *K*	69.16

(b) KNiF₃ powder

Element	Atomic%
K *K*	15.29
Ni *K*	12.22
F *K*	72.49

(c) AgNiF₃ powder

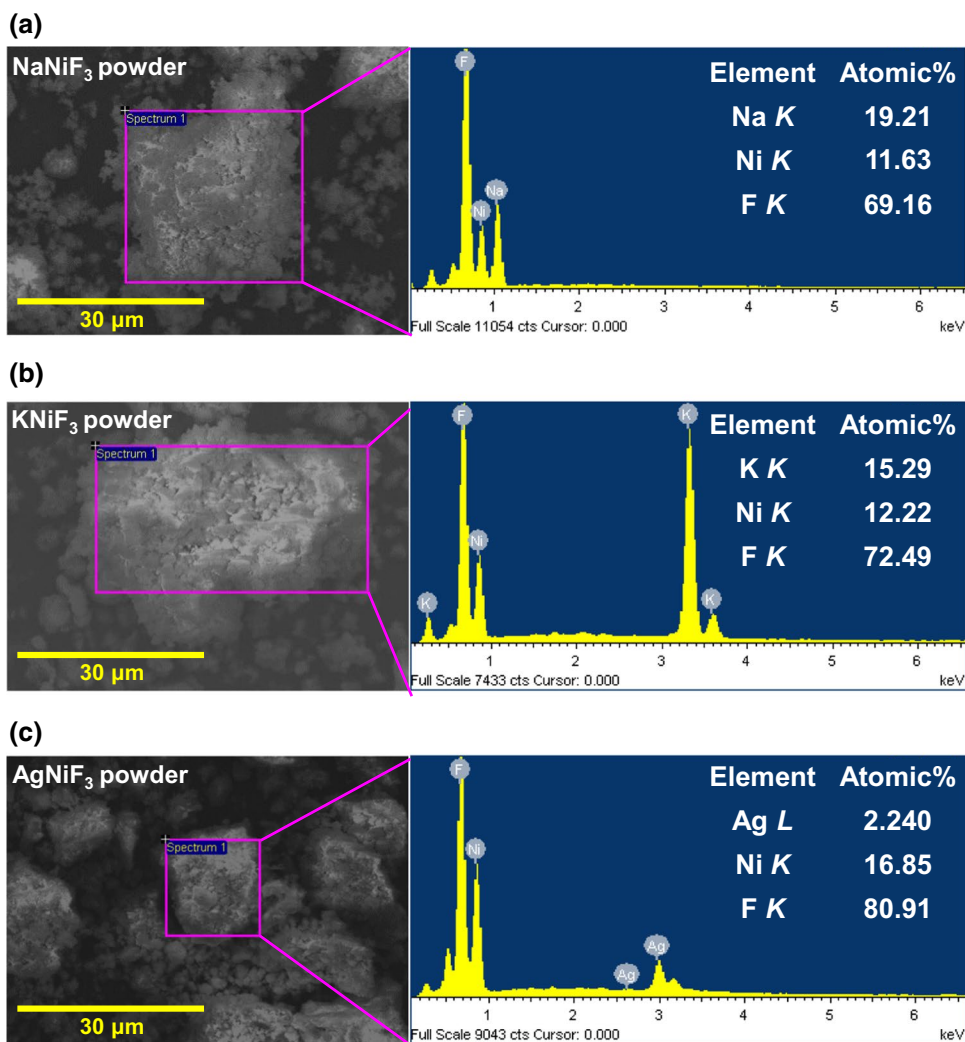| Element	Atomic%
Ag *L*	2.240
Ni *K*	16.85
F *K*	80.91

Table 3 Estimated lattice constants and goodness of fit via the Rietveld refinements of the XRD patterns of $AgNiF_3$ powders synthesized by methods 1 and 2. In these refinements, the crystal structures of $AgNiF_3$ were assumed to be cubic and orthorhombic separately for comparison

Material (structure)	Conventional mechanical grinding (method 1)		Planetary ball milling (method 2)	
	Lattice constant (Å)	Goodness of fit (χ^2)	Lattice constant (Å)	Goodness of fit (χ^2)
$AgNiF_3$ (cubic)	$a = 3.96$ $b = 3.96$ $c = 3.96$	3.07	$a = 3.96$ $b = 3.96$ $c = 3.96$	8.47
$AgNiF_3$ (orthorhombic)	$a = 3.83$ $b = 3.92$ $c = 3.93$	2.55	$a = 3.83$ $b = 3.92$ $c = 3.93$	2.45

changes to the orthorhombic structure (*Pnma*), resulting in a decrease in the tolerance factor [56–58]. We also emphasize that the more a perovskite material is structurally distorted, the more stabilization of the distorted perovskite phase becomes difficult [59]. Because fluoroperovskite $NaNiF_3$ is more distorted with an orthorhombic structure ($a = 5.38$ Å, $b = 5.55$ Å, and $c = 7.72$ Å for our $NaNiF_3$ powders) than cubic $KNiF_3$ ($a = b = c = 4.03$ Å for our $KNiF_3$ powders)

(Table 1), the synthesis of $NaNiF_3$ powders with a single perovskite phase would be quite difficult compared with perovskite $KNiF_3$.

An Ag deficiency in cubic perovskite $AgNiF_3$ may induce a structural transition from cubic symmetry to orthorhombic symmetry. We found that the XRD refinement results, where the perovskite structure in our Ag-deficient $AgNiF_3$ powders was assumed to be orthorhombic with different

Fig. 5 Rietveld refinement of the XRD patterns of AgNiF$_3$ ceramic powders prepared by methods 1 and 2. The XRD fitting results of our AgNiF$_3$ powders were performed under assumptions of the orthorhombic (**a**, **b**) and cubic (**c**, **d**) crystallographic structures. The observed XRD profiles of the ANiF$_3$ powder are represented by black circles. The XRD fitted lines of the calculated (Y_{cal}) and the difference between the observed and the calculated ($Y_{obs} - Y_{cal}$) XRD patterns are represented by red and blue lines, respectively
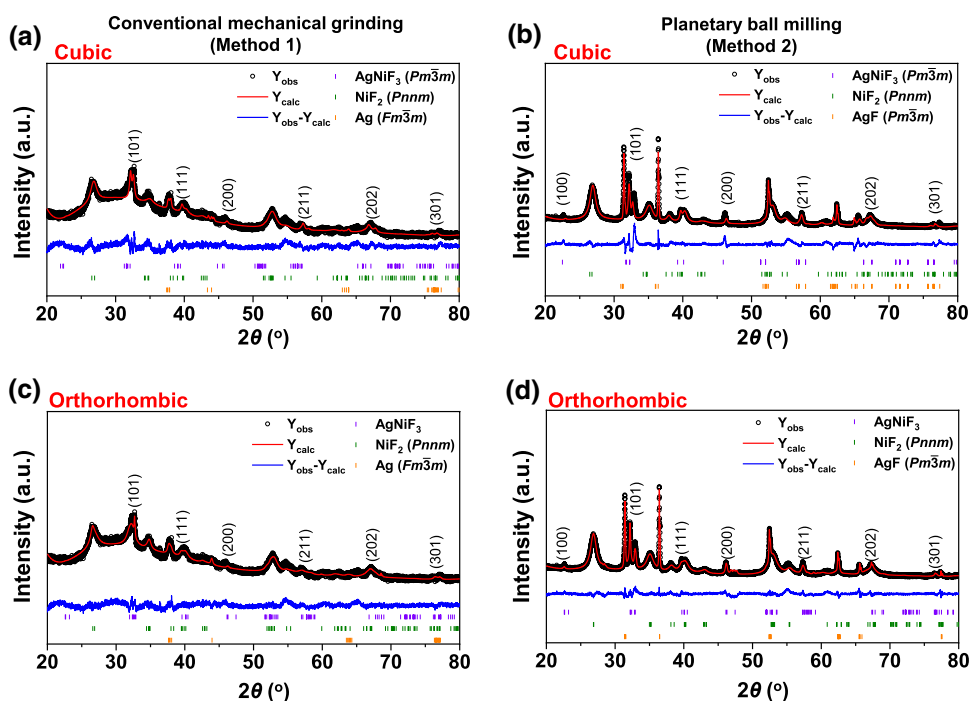
lattice constants ($a = 3.83$ Å, $b = 3.92$ Å, and $c = 3.93$ Å) with respect to all principal axes, gave a better goodness of factor ($\chi^2 = 2.45$) than the fitting results ($a = b = c = 3.96$ Å and $\chi^2 = 8.47$) derived from the assumption of cubic AgNiF$_3$ as in the bulk counterpart (Table 3). These XRD fitting results done by assuming two different crystal structures (orthorhombic and cubic) for our AgNiF$_3$ powders are shown in Fig. 5. Note that the crystallographic symmetry in perovskite materials is very susceptible to chemical stoichiometry [60]. In a cation-deficient perovskite A$_{1-x}$BX$_{3-\delta}$, the A-site cation and anion vacancies can be created for charge compensation [56, 60, 61]. With the formation of vacancy defects, a BX$_6$ octahedron is also distorted at the given vacancy site, leading to a structural phase transition locally [60, 62]. For instance, in the presence of cation vacancies, a cubic perovskite structure is transferred to an orthorhombic perovskite structure with lower crystallographic symmetry [63]. Thus, the perovskite phase in our Ag$_{1-x}$NiF$_{3-\delta}$ powders may be close to an orthorhombic rather than a cubic structure due to a structural distortion arising from the Ag deficiency. Because of the distorted orthorhombic structure, the fabrication of perovskite AgNiF$_3$ seems to be more challenging.

different synthetic procedures. We found the perovskite phase to be more easily formed in the fluoride perovskite powders synthesized by high-energy planetary ball milling than in those synthesized by conventional grinding. XRD refinement results revealed that the crystal structure of the perovskite AgNiF$_3$ powders was close to orthorhombic rather than cubic, unlike bulk AgNiF$_3$. This difference in the structural symmetry may be attributed to an octahedral distortion induced by Ag vacancies in Ag-deficient Ag$_{1-x}$NiF$_{3-\delta}$. Our work should be of potential interest for the synthesis of other perovskite halides (e.g., chlorides, bromides, and iodides) via a mechanochemical reaction. Furthermore, our synthetic approaches to Ni-based fluoroperovskites can be harnessed to realize experimentally infinite-layer fluoronickelates exhibiting superconductivity [64] and should allow high-efficiency fluoride electrodes to be achieved for lithium/sodium batteries [34].

4 Conclusion

In summary, we stabilized a perovskite phase in Ni-based fluoroperovskite ANiF$_3$ ($A =$ Na, K, and Ag) materials by two solvent-free mechanochemical reaction methods with

References

1. L.M. Feng, L.Q. Jiang, M. Zhu, H.B. Liu, X. Zhou, C.H. Li, J. Phys. Chem. Solids **69**, 967 (2008)

2. C. Li, X. Lu, W. Ding, L. Feng, Y. Gao, Z. Guo, Acta Cryst. B **64**, 702 (2008)

3. T. He, Q. Huang, A.P. Ramirez, Y. Wang, K.A. Regan, N. Rogado, M.A. Hayward, M.K. Haas, J.S. Slusky, K. Inumara, H.W. Zandbergen, N.P. Ong, R.J. Cava, Nature **411**, 54 (2001)

4. N. Reyren, S. Thiel, A.D. Caviglia, L.F. Kourkoutis, G. Hammerl, C. Richter, C.W. Schneider, T. Kopp, A.S. Ruetschi, D. Jaccard, M. Gabay, D.A. Muller, J.M. Triscone, J. Mannhart, Science **317**, 1196 (2007)

5. M. Imada, A. Fujimori, Y. Tokura, Rev. Mod. Phys. **70**, 1039 (1998)

6. J.B. Torrance, P. Lacorre, A.I. Nazzal, E.J. Ansaldo, C. Niedermayer, Phys. Rev. B Condens. Matter **45**, 8209 (1992)

7. H.J. Seog, A. Ullah, C.W. Ahn, I.W. Kim, S.Y. Lee, J. Park, H.J. Lee, S.S. Won, S.-H. Kim, J. Korean Phys. Soc. **72**, 1467 (2018)

8. A. Von Hippel, R. Breckenridge, F. Chesley, L. Tisza, Ind. Eng. Chem. **38**, 1097 (1946)

9. B.T. Nguyen, S.S. Won, B.C. Park, Y.J. Jo, C.W. Ahn, I.W. Kim, T.H. Kim, Curr. Appl. Phys. **20**, 1447 (2020)

10. H.J. Seog, B.C. Park, S. Cho, T.H. Kim, I.W. Kim, A. Ullah, New Phys. Sae Mulli **70**, 220 (2020)

11. B. Iaffe, R. Roth, S. Marzullo, J. Res. Natl. Bur. Stand. **55**, 239 (1955)

12. J. Wang, J.B. Neaton, H. Zheng, V. Nagarajan, S.B. Ogale, B. Liu, D. Viehland, V. Vaithyanathan, D.G. Schlom, U.V. Waghmare, N.A. Spaldin, K.M. Rabe, M. Wuttig, R. Ramesh, Science **299**, 1719 (2003)

13. T.K. Song, J.Y. Jo, S.M. Yang, D.H. Kim, S. Park, Y. Jo, J.-G. Yoon, J. Korean Phys. Soc. **56**, 503 (2010)

14. A. Weidenkaff, R. Robert, M. Aguirre, L. Bocher, T. Lippert, S. Canulescu, Renew. Energy **33**, 342 (2008)

15. L. Bocher, M.H. Aguirre, R. Robert, D. Logvinovich, S. Bakardjieva, J. Hejtmanek, A. Weidenkaff, Acta Mater. **57**, 5667 (2009)

16. A. Ramirez, J. Phys. Condens. Matter **9**, 8171 (1997)

17. Y. Inaguma, L.Q. Chen, M. Itoh, T. Nakamura, Solid State Ion. **70**, 196 (1994)

18. J. Mizusaki, K. Arai, K. Fueki, Solid State Ion. **11**, 203 (1983)

19. A. Kojima, K. Teshima, Y. Shirai, T. Miyasaka, J. Am. Chem. Soc. **131**, 6050 (2009)

20. H.-S. Kim, C.-R. Lee, J.-H. Im, K.-B. Lee, T. Moehl, A. Marchioro, S.-J. Moon, R. Humphry-Baker, J.-H. Yum, J.E. Moser, Sci. Rep. **2**, 1 (2012)

21. J. Suntivich, H.A. Gasteiger, N. Yabuuchi, H. Nakanishi, J.B. Goodenough, Y. Shao-Horn, Nat. Chem. **3**, 546 (2011)

22. T. Wang, H. Chen, Z. Yang, J. Liang, S. Dai, J. Am. Chem. Soc. **142**, 4550 (2020)

23. G. Koster, L. Klein, W. Siemons, G. Rijnders, J.S. Dodge, C.-B. Eom, D.H.A. Blank, M.R. Beasley, Rev. Mod. Phys. **84**, 253 (2012)

24. V.M. Goldschmidt, Berichte der deutschen chemischen Gesellschaft (A and B Series) **60**, 1263 (1927)

25. S. Catalano, M. Gibert, J. Fowlie, J. Iniguez, J.-M. Triscone, J. Kreisel, Rep. Prog. Phys. **81**, 046501 (2018)

26. Hayatullah, G. Murtaza, R. Khenata, S. Muhammad, A.H. Reshak, K.M. Wong, S.B. Omran, Z.A. Alahmed, Comput. Mater. Sci. **85**, 402 (2014)

27. Shakeel, A.H. Reshak, S. Khan, A. Laref, G. Murtaza, J. Bila, Opt. Mater. **109**, 110325 (2020)

28. S.A. Morley, H. Marquez, D. Lederman, APL Mater. **8**, 011101 (2020)

29. L. Yuan, L. Ge, X. Sun, J. Zhang, J. Yu, C. Zhang, H. Li, Cryst. Eng. Commun. **22**, 6216 (2020)

30. B.J. Garrard, B.M. Wanklyn, S.H. Smith, J. Cryst. Growth **22**, 169 (1974)

31. K. Yanagisawa, M. Yoshimura, S. Somiya, J. Mater. Sci. **17**, 177 (1982)

32. I.D. Gocheva, M. Nishijima, T. Doi, S. Okada, J.I. Yamaki, T. Nishida, J. Power Source **187**, 247 (2009)

33. M.R. Chierotti, A. Rossin, R. Gobetto, M. Peruzzini, Inorg. Chem. **52**, 12616 (2013)

34. E.C. Gonzalo, M.L. Sanjuan, M. Hoelzel, M.T. Azcondo, U. Amador, I. Sobrados, J. Sanz, F. Garcia-Alvarado, A. Kuhn, Inorg. Chem. **54**, 3172 (2015)

35. Y. Shirako, Y.G. Shi, A. Aimi, D. Mori, H. Kojitani, K. Yamaura, M. Akaogi, J. Solid State Chem. **191**, 167 (2012)

36. S.K. Valluri, I. Monk, M. Schoenitz, E.L. Dreizin, Int. J. Energ. Mater. Chem. Propuls. **16**, 81 (2017)

37. F.L. Bernal, K.V. Yusenko, J. Sottmann, C. Drathen, J. Guignard, O.M. Lovvik, W.A. Crichton, S. Margadonna, Inorg. Chem. **53**, 12205 (2014)

38. R.M. Gluck, T.H. Lee, F.T.J. Smith, Mater. Res. Bull. **9**, 305 (1974)

39. J. Lee, Q. Zhang, F. Saito, Chem. Lett. **30**, 700 (2001)

40. G. Scholz, ChemTexts **7**, 16 (2021)

41. *Faraday Discussion 170, Mechanochemistry: From Functional Solids to Single Molecules* (United Kingdom, Oxford, 2014).

42. P. Bala, *Mechanochemistry in Nanoscience and Minerals Engineering* (Germany, Berlin, 2008).

43. G. Kaupp, Cryst. Eng. Commun. **11**, 388 (2009)

44. L. Takacs, Acta Phys. Pol. A **126**, 1040 (2014)

45. Z. Hong, D. Tan, R.A. John, Y.K.E. Tay, Y.K.T. Ho, X. Zhao, T.C. Sum, N. Mathews, F. García, H.S. Soo, iScience **16**, 312 (2019)

46. L.B. McCusker, R.B. Von Dreele, D.E. Cox, D. Louër, P. Scardi, J. Appl. Crystallogr. **32**, 36 (1999)

47. H.M. Rietveld, Acta Crystallogr. **22**, 151 (1967)

48. H.M. Rietveld, J. Appl. Crystallogr. **2**, 65 (1969)

49. A. Kramida, Y. Ralchenko, J. Reader, N. A. Team, NIST Atomic Spectra Database, National Institute of Standards and Technology. https://physics.nist.gov/asd. Accessed 12 May 2021

50. A.V. Rane, K. Kanny, V.K. Abitha, S. Thomas, *Synthesis of Inorganic Nanomaterials* (England, Cambridge, 2018), Chap. 5, pp. 121–139

51. S. Körbel, M.A.L. Marques, S. Botti, J. Mater. Chem. C **4**, 3157 (2016)

52. D.E. Newbury, N.W.M. Ritchie, Scanning **35**, 141 (2013)

53. P.J. Statham, J. Res. Natl. Inst. Stand. Technol. **107**, 531 (2002)

54. P.M. Woodward, Acta. Crystallogr. B. Struct. Sci. Cryst. Eng. Mater. **53**, 44 (1997)

55. M.W. Lufaso, P.M. Woodward, Acta Crystallogr. Sect. B Struct. Sci. **57**, 725 (2001)

56. Y. Tokura, Y. Tomioka, J. Magn. Magn. Mater. **200**, 1 (1999)

57. Z. Liao, M. Huijben, Z. Zhong, N. Gauquelin, S. Macke, R.J. Green, S. Van Aert, J. Verbeeck, G. Van Tendeloo, K. Held, G.A. Sawatzky, G. Koster, G. Rijnders, Nat. Mater. **15**, 425 (2016)

58. D. Kan, R. Aso, R. Sato, M. Haruta, H. Kurata, Y. Shimakawa, Nat. Mater. **15**, 432 (2016)

59. S. Ogawa, J. Phys. Soc. Jpn. **15**, 2361 (1960)

60. S.A. Lee, H. Jeong, S. Woo, J.Y. Hwang, S.Y. Choi, S.D. Kim, M. Choi, S. Roh, H. Yu, J. Hwang, S.W. Kim, W.S. Choi, Sci. Rep. **6**, 23649 (2016)

61. J. Yeog Son, J.-H. Lee, H. Myung Jang, Appl. Phys. Lett. **103**, 102901 (2013)

62. F. Yang, Q. Zhang, Z. Yang, J. Gu, Y. Liang, W. Li, W. Wang, K. Jin, L. Gu, J. Guo, Appl. Phys. Lett. **107**, 082904 (2015)

63. U. Aschauer, R. Pfenninger, S.M. Selbach, T. Grande, N.A. Spaldin, Phys. Rev. B **88**, 054111 (2013)

64. F. Bernardini, V. Olevano, X. Blasé, A. Cano, J. Phys. Mater. **3**, 035003 (2020)
65. A. Okazaki, Y. Suemune, T. Fuchikami, J. Phys. Soc. Jpn. **14**, 1823 (1959)
66. L.Q. Jiang, J.K. Guo, H.B. Liu, M. Zhu, X. Zhou, P. Wu, C.H. Li, J. Phys. Chem. Solids **67**, 1531 (2006)

Publisher's Note Springer Nature remains neutral with regard to jurisdictional claims in published maps and institutional affiliations.